PROCEEDINGS OF SCIENCE

Renormalization constants of overlap quark bilinear operators from RI/MOM and RI/SMOM scheme

Fangcheng He[a] **and Yi-Bo Yang**[a,b,c,d,*]

[a] *CAS Key Laboratory of Theoretical Physics, Institute of Theoretical Physics, Chinese Academy of Sciences, Beijing 100190, China*

[b] *School of Fundamental Physics and Mathematical Sciences, Hangzhou Institute for Advanced Study, UCAS, Hangzhou 310024, China*

[c] *International Centre for Theoretical Physics Asia-Pacific, Beijing/Hangzhou, China*

[d] *School of Physical Sciences, University of Chinese Academy of Sciences, Beijing 100049, China*

E-mail: hefc123@itp.ac.cn, ybyang@itp.ac.cn

We calculate the renormalization constants (RCs) of vector, axial, vector scalar, pseudoscalar and tensor quark operators of the overlap valence fermion, on the 11 gauge ensembles with dynamical fermion using either Domain wall fermion (DWF) action or Highly improved stagger quark (HISQ) action at lattice spacings from 0.04 fm to 0.20 fm. We find the results under the $\overline{\text{MS}}$ scheme using either the RI/MOM or RI/SMOM scheme are consistent with each other, once the proper a^2p^2 extrapolation is and the systematic uncertainties are estimated cautiously. Our results with different gauge and fermion actions also indicate that the RCs are majorly dependent on the lattice spacing (as the inverse of UV cut-off) rather than the bare gauge coupling used by the gauge action.

The 38th International Symposium on Lattice Field Theory, LATTICE2021 26th-30th July, 2021 Zoom/Gather@Massachusetts Institute of Technology

*Speaker

PoS(LATTICE2021)610

1. Introduction

RI/MOM [1] and RI/SMOM [2, 3] schemes are widely used to renormalize the bare matrix element calculated by Lattice QCD. In the RI/MOM scheme, the vertex correction is considered in the forward off-shell parton state. The momenta of external quark legs are chosen to be $p_1 = p_2 = p$ with the renormalization scale μ defined by $\mu^2 = p^2$, and the RCs are determined by the following renormalization conditions [1],

$$\begin{aligned} Z_q^{\mathrm{RI/MOM}} &= \lim_{m_R\to 0} \frac{-i}{48}\mathrm{Tr}\Big[\gamma_\mu \frac{\partial S_B^{-1}(p)}{\partial p_\mu}\Big]_{p^2=\mu^2}, \\ Z_O^{\mathrm{RI/MOM}} &= \lim_{m_R\to 0} \frac{Z_q^{\mathrm{RI/MOM}}}{\frac{1}{12}\mathrm{Tr}[\Lambda_{O,B}(p,p)\Lambda_O^{\mathrm{tree}}(p,p)^{-1}]}\Big|_{p^2=\mu^2}. \end{aligned} \tag{1a}$$

However, the definition in Eq. (1a) introduces the derivative to the momentum, which is cumbersome to fulfill in the discretized lattice. A better choice to obtain $Z_q^{\mathrm{RI/MOM}}$ is through the vector vertex correction

$$Z_q^{\mathrm{RI/MOM}} = \lim_{m_R\to 0} \frac{Z_V^{\mathrm{RI/MOM}}}{12}\mathrm{Tr}[\Lambda^\mu_{V,B}(p,p)\gamma_\mu], \tag{2}$$

where $\Lambda_{V,B}(p)$ is the bare vector vertex. Thus the RCs of arbitrary quark bi-linear operators O can be obtained through

$$Z_O^{\mathrm{RI/MOM}} = Z_V^{\mathrm{RI/MOM}} \lim_{m_R\to 0} \frac{\mathrm{Tr}[\Lambda_{V,B}(p,p)\gamma_\mu]}{\mathrm{Tr}[\Lambda_{O,B}(p,p)\Lambda_O^{\mathrm{tree}}(p,p)^{-1}]}\Big|_{p^2=\mu^2}. \tag{3}$$

In the RI/SMOM scheme, the momenta of external quark legs are systematically set to be

$$p_1^2 = p_2^2 = (p_2 - p_1)^2 = \mu^2. \tag{4}$$

The renormalization conditions for the quark self energy, scalar, pseudoscalar, tensor, vector and axial vector currents are chosen to be [2, 3]

$$Z_q^{\mathrm{RI/SMOM}} = \lim_{m_R\to 0} \frac{-i}{12p^2}\mathrm{Tr}\Big[S_B^{-1}(p)\not{p}\Big]_{p^2=\mu^2}, \tag{5a}$$

$$Z_{S/P/T}^{\mathrm{RI/SMOM}} = \lim_{m_R\to 0} \frac{Z_q^{\mathrm{RI/SMOM}}}{\frac{1}{12}\mathrm{Tr}[\Lambda_{S/P/T,B}(p_1,p_2)\Lambda_{S/P/T}^{\mathrm{tree}}(p_1,p_2)^{-1}]}, \tag{5b}$$

$$Z_V^{\mathrm{RI/SMOM}} = \lim_{m_R\to 0} \frac{Z_q^{\mathrm{RI/SMOM}}}{\frac{1}{12q^2}\mathrm{Tr}[q_\mu\Lambda^\mu_{V,B}(p_1,p_2)\not{q}]}, \tag{5c}$$

$$Z_A^{\mathrm{RI/SMOM}} = \lim_{m_R\to 0} \frac{Z_q^{\mathrm{RI/SMOM}}}{\frac{1}{12q^2}\mathrm{Tr}[q_\mu\Lambda^\mu_{A,B}(p_1,p_2)\gamma_5\not{q}]}. \tag{5d}$$

If one use Eq. (5a) to calculate the $Z_q^{\mathrm{RI/SMOM}}$ in the lattice, the result will suffer large discretization error [4]. Thus we can follow the similar strategy used by the RI/MOM scheme, and use the following vector current correction to obtain the $Z_q^{\mathrm{RI/SMOM}}$,

$$Z_q^{\mathrm{RI/SMOM}} = \lim_{m_R\to 0} \frac{Z_V^{\mathrm{RI/SMOM}}}{12}\mathrm{Tr}[q_\mu\Lambda^\mu_{V,B}(p_1,p_2)\not{q}]_{sym}, \tag{6}$$

then define RCs of other quark operator as

$$Z_O^{\mathrm{RI/SMOM}} = Z_V^{\mathrm{RI/SMOM}} \lim_{m_R \to 0} \frac{\mathrm{Tr}[q_\mu \Lambda^\mu_{V,B}(p_1,p_2) \not{q}]}{\mathrm{Tr}[\Lambda_{O,B}(p_1,p_2)\Lambda_O^{\mathrm{tree}}(p_1,p_2)^{-1}]}\Big|_{p^2=\mu^2}. \tag{7}$$

In this work, we use both the RI/MOM and RI/SMOM schemes as the intermediate schemes to renormalize the current quark operators on the several gauge ensembles. The gauge ensembles use the dynamical Domain wall fermion (DWF) action and Symanzik gauge action [5, 6] with the bare guage coupling $6/g^2 \sim 2$, or Highly improved stagger quark (HISQ) actions and Iwasaki gauge action [7] with the bare guage coupling $6/g^2 \sim 4$. The information of these gauge ensembles are listed in the Table. (1).

To suppress the discretization error, the momenta are chosen to be close the body diagonal in the RI/MOM scheme, i.e.,

$$\frac{p^{[4]}}{(p^2)^2} < 0.28, \text{where } p^{[4]} = \sum_\mu p_\mu^4,\ p^2 = \sum_\mu p_\mu^2. \tag{8}$$

In the RI/SMOM scheme, the momenta is chosen to be symmetrical form, such as p_1=(q,q,0,0), p_2=(0,q,q,0). The results in the RI/MOM and RI/SMOM can be converted to the $\overline{\mathrm{MS}}$ scheme by using the perturbative matching factors, which can be found in [8–12]. Then we use the anomalous dimension to evolve the results to 2 GeV. The final results can be obtained by applying appropriate ansatz to extrapolate the results to $a^2p^2 \to 0$ limit. In Fig. 1, we present our results about $Z_S^{\overline{\mathrm{MS}}}$(2GeV) on the different gauge ensembles from RI/MOM (red data points) and RI/SMOM schemes (blue data points). The rectangle and circle represent the results on the HISQ ensemble and DWF ensembles. We can see that the result is a smooth function of the lattice spacing, rather than $6/g^2$ which can be sensitive to the used gauge action.

tag	$6/g^2$	L	T	a(fm)	m_π (MeV)
HISQ12	3.60	24	64	0.1213(9)	310
HISQ09	3.78	32	96	0.0882(7)	310
HISQ06	4.03	48	144	0.0574(5)	310
HISQ04	4.20	64	192	0.0425(4)	310
24D	1.633	24	64	0.194(2)	139
24DH	1.633	24	64	0.194(2)	337
32Dfine	1.75	32	64	0.143(2)	139
48I	2.13	48	96	0.1141(2)	139
64I	2.25	64	128	0.0837(2)	139
48If	2.31	48	96	0.0711(3)	280
32If	2.37	32	64	0.0626(4)	371

Table 1: Setup of the ensembles, including the bare coupling constant g, lattice size $L^3 \times T$, lattice spacing a and sea pion mass m_π.

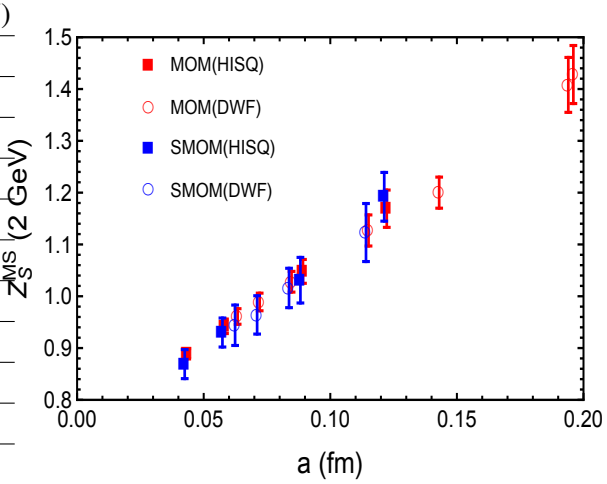

Figure 1: $Z_S^{\overline{\mathrm{MS}}}$(2GeV) calculated with intermediate RI/MOM and RI/SMOM results on the different gauge ensembles we used.

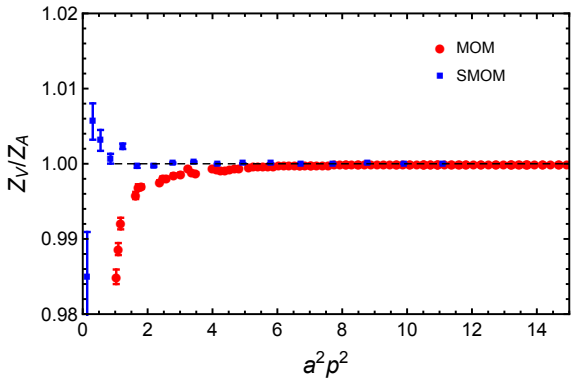

Figure 2: The ratio Z_V/Z_A in the chiral limit in the RI/MOM and RI/SMOM scheme.

2. Numerical details

In this section, we choose the RCs on the 48I ensemble to show the updated analysis with a larger p^2 range, as those RCs have been calculated in the previous χQCD work [14].

2.1 Renormalization of vector current and axial vector current

The RC of axial vector current can be calculated through the PCAC relation,

$$Z_A\partial_\mu(\bar{\psi}\gamma_5\gamma_\mu\psi) = 2Z_mZ_Pm_q\bar{\psi}\gamma_5\psi = 2m_q\bar{\psi}\gamma_5\psi, \tag{9}$$

since Z_mZ_P=1 for the overlap fermions. In Fig. 2, we present the ratio of Z_V/Z_A in the RI/MOM and RI/SMOM scheme, and it is clear that $Z_V/Z_A = 1$ are well satisfied both in the RI/MOM and RI/SMOM scheme, as we expect for the chiral fermion. Except the statistical error, we also estimate systematic errors cause by the finite volume effect and non-zero strange quark in the gauge ensemble, more details can be found in our upcoming paper [13]. The final results of Z_A on different ensembles are shown in Table. 2.

Ensemble	HISQ12	HISQ09	HISQ06	HISQ04
Z_A	1.1102(2)(1)(18)	1.0834(1)(1)(20)	1.0617(1)(1)(20)	1.0523(1)(1)(19)
Ensemble	48I	64I	48If	32If
Z_A	1.1037(1)(1)(21)	1.0787(1)(1)(19)	1.0700(1)(1)(18)	1.0646(2)(2)(19)
Ensemble	24D	24DH	32Dfine	
Z_A	1.2193(3)(1)(27)	1.2251(3)(1)(27)	1.1417(2)(1)(20)	

Table 2: The renormalization constants axial current on the different ensembles. The values in the three brackets following the center value correspond to the statistical error, systematic errors caused by the finite volume effect and non-zero strange quark mass.

2.2 Renormalization of quark self energy

The RCs of quark field strength in the RI/MOM and RI/SMOM schemes can be obtained the vector current vertex correction in Eq. (2) and Eq. (6). Using perturbative matching factors, one

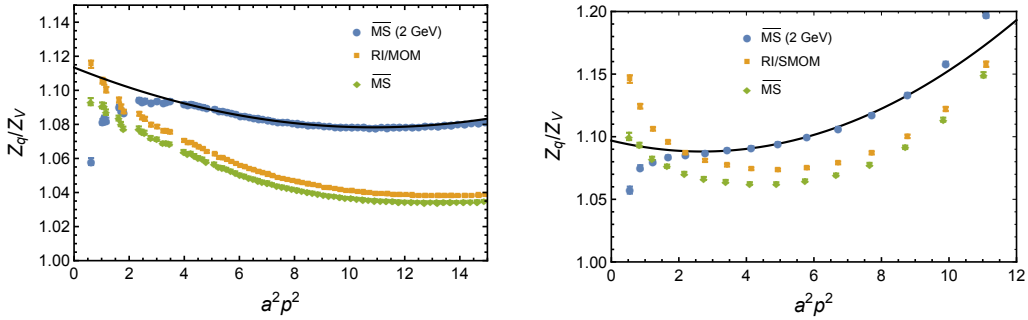

(a) (b)

Figure 3: The conversion of Z_q/Z_V in the RI/MOM scheme (left panel) and RI/SMOM scheme (right panel) to the $\overline{\text{MS}}$ schemes. The results at 2GeV are obtained using the anomalous dimension of quark field strength in the $\overline{\text{MS}}$ scheme. The solid lines represent the extrapolation of a^2p^2 with Eq. (10) using the data in the specific region we mention in the text.

can convert the RCs in the intermediate schemes to the $\overline{\text{MS}}$ scheme. These results are presented in Fig. (3). To remove the discretiztion error, we use the following ansatz to fit the data

$$f = c_0 + c_1 a^2p^2 + c_2(a^2p^2)^2, \tag{10}$$

the fit regions for the results from RI/MOM scheme and RI/SMOM are chosen to be $a^2p^2 \in [6:12]$ and $a^2p^2 \in [2.5:9]$, respectively. The corrsepoding fit results for c_0 are 1.1142(27) and 1.0969(38). In addition to the statistical error, we should also consider the systematical error caused by the fit region of a^2p^2, perturbative matching factors, finite volume effect, non-zero strange quark and the uncertainties of Λ_{QCD} and lattice spacing, etc, and the details will be presented in [13, 14]. The final results for the $Z_q^{\overline{\text{MS}}}(2\text{ GeV})/Z_V$ from the intermediate RI/MOM and RI/SMOM are consistent, which are 1.114(5) and 1.097(23). The most uncertainty in the RI/MOM and RI/SMOM schemes are from the truncation error in the perturbative matching from the RI/MOM scheme to $\overline{\text{MS}}$ scheme and the fit region of a^2p^2 in the a^2p^2 extrapolation, respectively.

2.3 Renormalization of scalar and pseudoscalar quark operator

There are unphysical mass poles in the forward scalar and pseudoscalar quark matrix elements, they correspond to the contribution from the zero mode of Dirac operator [15] and goldstone mass pole [1] in the chiral limit. In Fig. 4, we present the quark mass dependence for the RCs of scalar quark and pseudoscalar quark operators in RI/MOM and RI/SMOM schemes. One can see that $Z_S^{\text{RI/MOM}}$ and $Z_P^{\text{RI/MOM}}$ are very sensitive to the valence quark mass. We use the following ansatz to extrapolate the results to the chiral limit,

$$Z_S^{\text{RI/MOM}}/Z_A(am_q) = \frac{A_s}{(am_q)^2} + B_s + C_s am_q, \qquad Z_P^{\text{RI/MOM}}/Z_A(am_q) = 1/\left\{\frac{A_p}{(am_q)} + B_p + C_p am_q\right\}, \tag{11}$$

where B_s and $1/B_p$ are the results of $Z_S^{\text{RI/MOM}}/Z_V$ and $Z_P^{\text{RI/MOM}}/Z_V$ in the chiral limit. The contamination of both the zero mode and goldstone pole are much smaller in the RI/SMOM scheme, it allows us to choose the linear chiral extrapolation.

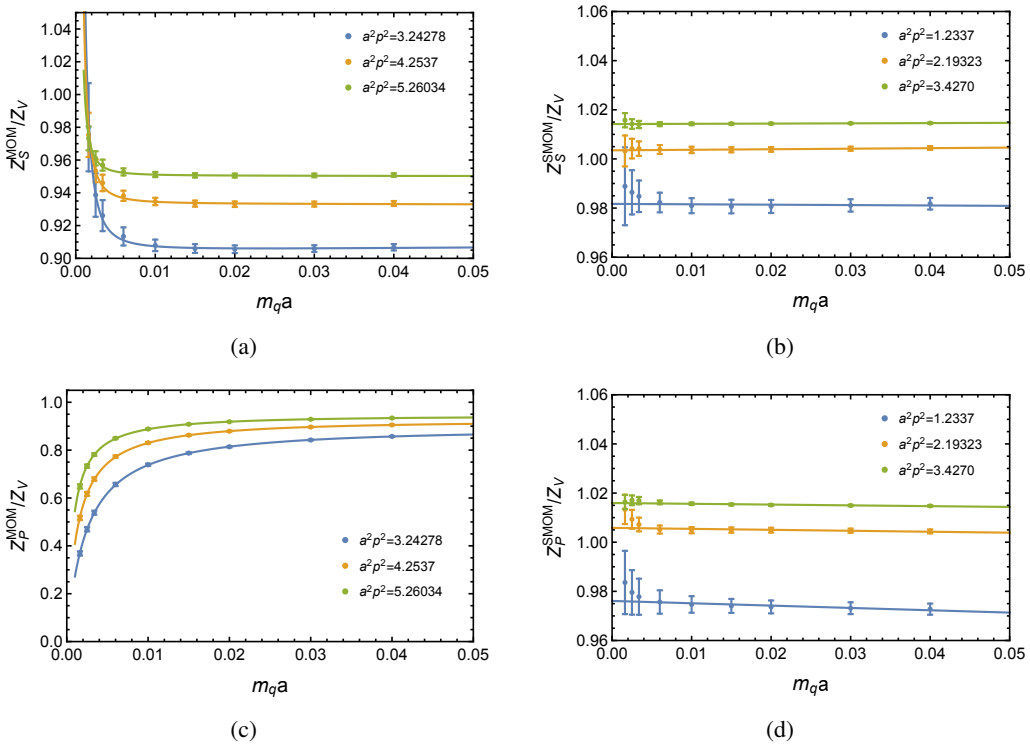

Figure 4: The quark mass dependence for the Z_S/Z_V and Z_P/Z_V in the RI/MOM scheme and RI/SMOM schemes.

The conversion of Z_S/Z_V from the intermediate schemes to the $\overline{\text{MS}}$ scheme are presented in Fig. 5. One can see that the RI/SMOM scheme has better convergence of the perturbative matching than the RI/MOM scheme. However, after converting to the $\overline{\text{MS}}$ and running to 2 GeV, the results from the RI/SMOM scheme have very non-linear dependence on a^2p^2, but that $Z_S^{\overline{\text{MS}}}(2\text{GeV})/Z_A$ calculated with the RI/MOM scheme are almost linear on a^2p^2 when $4 \leq a^2p^2$. Using the fit ansatz in Eq. (10) to fit the data in $a^2p^2 \in [6:12]$ from the RI/MOM scheme, we obtain $Z_S^{\overline{\text{MS}}}(2\text{GeV})/Z_A$ is 1.0208(29). When we use Eq. (10) to fit the results from the RI/SMOM scheme, we find the largest fit region we can use is $a^2p^2 \in [4:9]$ if the upper limit is fixed and the constraint $\chi^2/d.o.f \leq 1$ is applied. The corresponding fit result is $Z_S^{\overline{\text{MS}}}(2\text{GeV})/Z_A = 1.0179(25)$. In addition, we also consider the following empirical form to fit the result from RI/SMOM scheme,

$$f = \frac{c_1}{a^2p^2} + c_0 + c_1 a^2p^2 + c_2(a^2p^2)^2, \tag{12}$$

then the fit range can be extended to be $a^2p^2 \in [1:9]$ with $\chi^2/d.o.f = 0.6$ after $1/(a^2p^2)$ term is included, and the corresponding fit result for c_0 is 0.9652(44). We take the deviation between results obtained by two different fit models as the systematic error. We also considered the uncertainty caused by the other sources as we mention in the Sec. (2.2). The final results for $Z_S^{\overline{\text{MS}}}$ is 1.127(30) and 1.123(58) from the RI/MOM and the RI/SMOM schemes. The most uncertainty is contributed by the truncation error in the matching factor for the RI/MOM scheme and the deviation between different fit models for the RI/SMOM scheme.

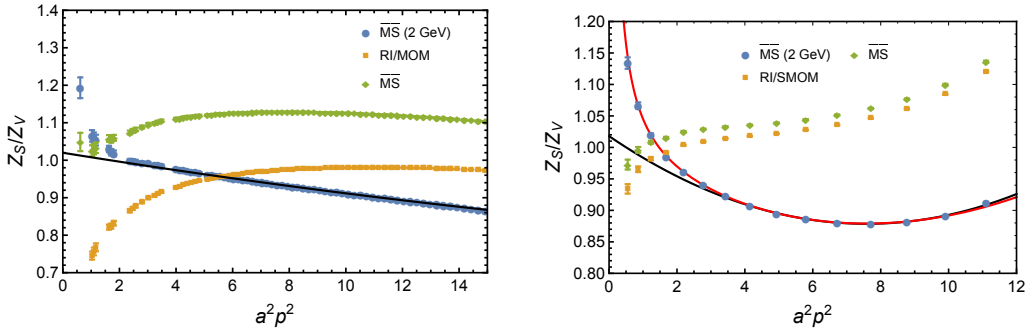

(a) (b)

Figure 5: Conversion and running of Z_S/Z_V for the intermediate schemes RI/MOM and RI/SMOM schemes. The black curves are the fittings using Eq. (10), the red curve in the right panel is the fitting with Eq. (12).

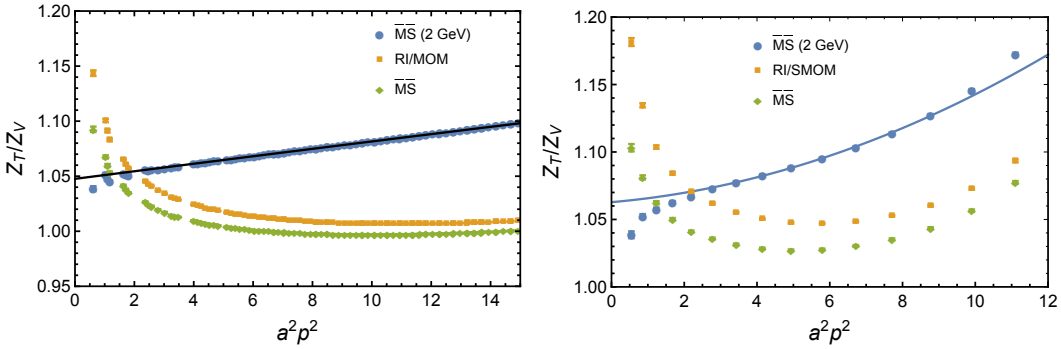

(a) (b)

Figure 6: Similar as Fig. 3 but for Z_T/Z_V.

2.4 Renormalization of tensor quark operator

The results of $Z_T^{\overline{\text{MS}}}(2\text{GeV})/Z_V$ from the RI/MOM and RI/SMOM are presented in Fig. 6. The results from RI/MOM scheme show a linear dependence on the a^2p^2. And we also choose Eq. (10) to fit data in $a^2p^2 \in [6:12]$ and $a^2p^2 \in [2.5:9]$ for the results from the RI/MOM and RI/SMOM schemes, respectively. The fit results we obtained are 1.0486(5) and 1.0628(23). Contracted to the scalar operator case, Z_T using RI/MOM scheme shows a better perturbative convergence than that using the RI/SMOM scheme. After considering all the systematic error, our results about $Z_T^{\overline{\text{MS}}}(2\text{GeV})$ is about 1.158(1) and 1.173(18). The uncertainty of results from RI/MOM scheme is small and the most uncertainty in the result from RI/SMOM scheme is caused by the different fit region of a^2p^2.

3. Conclusion

In this work, we renormalize the bare matrix elements of vector, axial vector, scalar, pseudoscalar and tensor quark operators calculated with valence overlap fermion on the dynamical DWF

and HISQ gauge ensembles. Using the perturbative matching factors and anomalous dimensions, we convert the results from the intermediate RI/MOM and RI/SMOM schemes to the $\overline{\text{MS}}$ 2 GeV. In addition the statistical error, we also consider kinds of systematic errors in the final results. We find the intermediate RI/MOM and RI/SMOM schemes can provide consistent results after converting to the $\overline{\text{MS}}$ scheme and doing appropriate a^2p^2 extrapolation. The RI/SMOM scheme show better perturbative convergence when matching to the $\overline{\text{MS}}$ scheme for the scalar quark operator, the case is opposite for the tensor quark operator, the perturbative series have better convergence for the RI/MOM scheme. After converting the results to 2 GeV, the results from RI/MOM scheme show better linear dependence on a^2p^2. The results from RI/SMOM scheme show obvious non-linear dependence on a^2p^2, it leads to a huge dependence on the a^2p^2 fit region. For the scalar operator, we use two different fit models to describe the data and fit results between these fit models have obvious deviation, while the deviation decreases slowly on the lattice spacing.

In Table 3, we list the RCs of different quark operators on the 11 gauge ensembles. We would like to mention that the lattice spacing of 24D, 24DH and 32Dfine are too large to calculate in RI/SMOM scheme. One can see that the final results from RI/MOM and RI/SMOM schemes are all consistent within the uncertainties.

4. Ackonwledge

We thank the RBC and UKQCD collaborations for providing us their DWF gauge configurations, and MILC collaboration for providing the HISQ gauge configurations. The calculations were performed using the GWU code [16, 17] through HIP programming model [18]. The numerical calculation is supported by the Strategic Priority Research Program of Chinese Academy of Sciences, Grant No. XDC01040100, and also the supercomputing system in the Southern Nuclear Science Computing Center (SNSC).

	Results from the RI/MOM scheme				Results from the RI/SMOM scheme			
Ensemble	Z_q(2GeV)	Z_S(2GeV)	Z_P(2GeV)	Z_T(2GeV)	Z_q(2GeV)	Z_S(2GeV)	Z_P(2GeV)	Z_T(2GeV)
HISQ12	1.246(7)	1.169(36)	1.230(63)	1.159(3)	1.230(20)	1.192(47)	1.151(41)	1.173(15)
HISQ09	1.204(5)	1.048(23)	1.062(28)	1.152(3)	1.184(28)	1.031(44)	1.028(38)	1.160(22)
HISQ06	1.169(7)	0.942(14)	0.944(22)	1.156(3)	1.163(20)	0.930(28)	0.931(29)	1.165(16)
HISQ04	1.154(6)	0.889(10)	0.890(18)	1.163(4)	1.144(15)	0.869(28)	0.871(26)	1.167(15)
24D	1.364(24)	1.408(53)	1.427(62)	1.230(7)	—	—	—	—
24DH	1.369(23)	1.428(56)	1.454(75)	1.236(7)	—	—	—	—
32Dfine	1.254(13)	1.200(30)	1.208(37)	1.181(2)	—	—	—	—
48I	1.230(6)	1.127(30)	1.140(35)	1.158(3)	1.211(25)	1.123(58)	1.127(51)	1.173(18)
64I	1.198(5)	1.028(20)	1.032(26)	1.152(2)	1.179(29)	1.016(38)	1.017(37)	1.165(20)
48If	1.182(6)	0.989(17)	0.997(23)	1.152(2)	1.168(23)	0.964(37)	0.966(41)	1.163(18)
32If	1.169(6)	0.961(15)	0.964(21)	1.155(3)	1.156(15)	0.944(39)	0.944(44)	1.160(12)

Table 3: The RCs of quark sele energy, scalar operator, pesudoscalar operator and tensor operator in $\overline{\text{MS}}$ scheme and 2 GeV from the RI/MOM and RI/SMOM schemes.

References

[1] G. Martinelli, C. Pittori, C. T. Sachrajda, M. Testa, and A. Vladikas *Nucl. Phys.* **B445** (1995) 81–108, arXiv:hep-lat/9411010 [hep-lat].

[2] Y. Aoki *et al.* *Phys. Rev.* **D78** (2008) 054510, arXiv:0712.1061 [hep-lat].

[3] C. Sturm, Y. Aoki, N. H. Christ, T. Izubuchi, C. T. C. Sachrajda, and A. Soni *Phys. Rev.* **D80** (2009) 014501, arXiv:0901.2599 [hep-ph].

[4] L. Chang, Y.-B. Liu, K. Raya, J. Rodríguez-Quintero, and Y.-B. Yang *Phys. Rev. D* **104** no. 9, (2021) 094509, arXiv:2105.06596 [hep-lat].

[5] **RBC, UKQCD** Collaboration, T. Blum *et al.* *Phys. Rev. D* **93** no. 7, (2016) 074505, arXiv:1411.7017 [hep-lat].

[6] P. A. Boyle *et al.* *Phys. Rev. D* **93** no. 5, (2016) 054502, arXiv:1511.01950 [hep-lat].

[7] **MILC** Collaboration, A. Bazavov *et al.* *Phys. Rev. D* **87** no. 5, (2013) 054505, arXiv:1212.4768 [hep-lat].

[8] E. Franco and V. Lubicz *Nucl. Phys. B* **531** (1998) 641–651, arXiv:hep-ph/9803491.

[9] K. G. Chetyrkin and A. Retey *Nucl. Phys.* **B583** (2000) 3–34, arXiv:hep-ph/9910332 [hep-ph].

[10] L. G. Almeida and C. Sturm *Phys. Rev. D* **82** (2010) 054017, arXiv:1004.4613 [hep-ph].

[11] J. A. Gracey *Eur. Phys. J. C* **71** (2011) 1567, arXiv:1101.5266 [hep-ph].

[12] B. A. Kniehl and O. L. Veretin *Phys. Lett. B* **804** (2020) 135398, arXiv:2002.10894 [hep-ph].

[13] F. He, Y. Bi, T. Draper, K.-F. Liu, Z. Liu, and Y.-B. Yang (in preparation).

[14] Y. Bi, H. Cai, T. Draper, M. Gong, K.-F. Liu, Z. Liu, and Y.-B. Yang *Phys. Rev.* **D97** no. 9, (2018) 094501, arXiv:1710.08678 [hep-lat].

[15] T. Blum *et al.* *Phys. Rev. D* **66** (2002) 014504, arXiv:hep-lat/0102005.

[16] A. Alexandru, C. Pelissier, B. Gamari, and F. Lee *J. Comput. Phys.* **231** (2012) 1866–1878, arXiv:1103.5103 [hep-lat].

[17] A. Alexandru, M. Lujan, C. Pelissier, B. Gamari, and F. X. Lee in *Proceedings, 2011 Symposium on Application Accelerators in High-Performance Computing (SAAHPC'11): Knoxville, Tennessee, July 19-20, 2011*, pp. 123–130. 2011. arXiv:1106.4964 [hep-lat].

[18] Y.-J. Bi, Y. Xiao, W.-Y. Guo, M. Gong, P. Sun, S. Xu, and Y.-B. Yang *PoS* **LATTICE2019** (2020) 286, arXiv:2001.05706 [hep-lat].